



CHORUS

This is the accepted manuscript made available via CHORUS. The article has been published as:

Giant nonlinearity via breaking parity-time symmetry: A route to low-threshold phonon diodes

Jing Zhang, Bo Peng, Şahin Kaya Özdemir, Yu-xi Liu, Hui Jing, Xin-you Lü, Yu-long Liu, Lan Yang, and Franco Nori

Phys. Rev. B **92**, 115407 — Published 8 September 2015

DOI: [10.1103/PhysRevB.92.115407](https://doi.org/10.1103/PhysRevB.92.115407)

Giant nonlinearity via breaking parity-time symmetry: a route to low-threshold phonon diodes

Jing Zhang,^{1,2,3,*} Bo Peng,³ Şahin Kaya Özdemir,^{3,†} Yu-xi Liu,^{4,2,‡} Hui Jing,^{5,6} Xin-you Lü,^{7,6} Yu-long Liu,⁴ Lan Yang,^{3,§} and Franco Nori^{6,8,¶}

¹*Department of Automation, Tsinghua University, Beijing 100084, P. R. China*

²*Center for Quantum Information Science and Technology, TNList, Beijing 100084, P. R. China*

³*Department of Electrical and Systems Engineering, Washington University, St. Louis, MO 63130, USA*

⁴*Institute of Microelectronics, Tsinghua University, Beijing 100084, P. R. China*

⁵*Department of Physics, Henan Normal University, Xinxiang 453007, P. R. China*

⁶*CEMS, RIKEN, Saitama 351-0198, Japan*

⁷*School of physics, Huazhong University of Science and Technology, Wuhan 430074, China*

⁸*Physics Department, The University of Michigan, Ann Arbor, MI 48109-1040, USA*

Nonreciprocal devices that permit wave transmission in only one direction are indispensable in many fields of science including, e.g., electronics, optics, acoustics, and thermodynamics. Manipulating phonons using such nonreciprocal devices may have a range of applications such as phonon diodes, transistors, switches, etc. One way of achieving nonreciprocal phononic devices is to use materials with strong nonlinear response to phonons. However, it is not easy to obtain the required strong mechanical nonlinearity, especially for few-phonon situations. Here, we present a general mechanism to amplify nonlinearity using \mathcal{PT} -symmetric structures, and show that an on-chip micro-scale phonon diode can be fabricated using a \mathcal{PT} -symmetric mechanical system, in which a lossy mechanical-resonator with very weak mechanical nonlinearity is coupled to a mechanical resonator with mechanical gain but no mechanical nonlinearity. When this coupled system transits from the \mathcal{PT} -symmetric regime to the broken- \mathcal{PT} -symmetric regime, the mechanical nonlinearity is transferred from the lossy resonator to the one with gain, and the effective nonlinearity of the system is significantly enhanced. This enhanced mechanical nonlinearity is almost lossless because of the gain-loss balance induced by the \mathcal{PT} -symmetric structure. Such an enhanced lossless mechanical nonlinearity is then used to control the direction of phonon propagation, and can greatly decrease (by over three orders of magnitude) the threshold of the input-field intensity necessary to observe the unidirectional phonon transport. We propose an experimentally realizable lossless low-threshold phonon diode of this type. Our study opens up new perspectives for constructing on-chip few-phonon devices and hybrid phonon-photon components.

I. INTRODUCTION

Owing to recent progress in nanotechnology and materials science, nano- and micro-mechanics¹⁻⁷ have emerged as subjects of great interest due to their potential use in demonstrating macroscopic quantum phenomena, and possible applications in precision measurements, detecting gravitational waves, building filters, signal amplification, as well as switches and logic gates. In particular, on-chip single- or few-phonon devices are ideal candidates for hybrid quantum information processing, due to the ability of phonons to interact and rapidly switch between optical fields and microwave fields^{8,9}. Fabrication of high-frequency mechanical resonators¹⁰, demonstration of coherent phonon coupling between nanomechanical resonators¹¹, ground-state cooling^{12,13}, optomechanics (in microtoroids^{14,15}, microspheres¹⁶⁻¹⁸, microdisks¹⁹⁻²¹, microring²², photonic crystals¹¹, doubly- or singly-clamped cantilevers^{23,24}, and membranes²⁵) have opened new directions⁵ and provided new tools to control and manipulate phonons in on-chip devices. One possible obstacle to further develop this field is the ability to control the flow of phonons, allowing transport in one direction but not the opposite direction²⁶, i.e., nonrecipro-

cal phonon transport. There have been several attempts to fabricate nonreciprocal devices for phonons²⁷⁻³², but these are almost exclusively based on asymmetric linear structures which indeed cannot break Lorentz reciprocity: a static linear structure cannot break reciprocity²⁷. These proposed linear structures do obey the reflection-transmission reciprocity and thus cannot be considered as “phonon diodes”. Diode-like behavior was observed in these linear acoustic structures because the input-output channels were not properly switched²⁷.

Nonreciprocal phonon transmission inevitably requires magneto-acoustic materials, strong nonlinearity, or a time-dependent modulation of the parameters of a structure. Although already demonstrated in optics³³, the time-dependent modulation of acoustic parameters of a phononic structure has not been probed yet. Magneto-acoustic materials require high magnetic fields to operate and have been studied³⁴; however, a magnetic-free nonreciprocal device is critical for building on-chip and small-scale phononic processors and circuits. Nonlinearity-based nonreciprocity seems to be the most viable approach for creating micro- or nano-scale nonreciprocal devices for controlling and manipulating phonons.

Recently, there have been several reports on nonlinear mechanical structures and materials³⁵⁻³⁸. However, the

weak nonlinearity of those acoustic/phononic materials hinders progress in this direction due to the high input powers required to observe the nonlinear effects^{39,40}. In order to circumvent this problem, coupling a weakly nonlinear structure to an auxiliary system, such as a quantum bit⁴¹, has been proposed to engineer effective giant mechanical nonlinearities.

In order to achieve the required nonlinearity for non-reciprocal phonon transport and to study nonlinear phononics, here we introduce a new method based on parity-time (\mathcal{PT}) symmetry⁴², which has attracted much attention recently due to their interesting and generally counter-intuitive physics^{43–68}. Parity-time symmetry and its breaking (broken \mathcal{PT} -phase) have been demonstrated in various physical systems^{52–64}, such as optical waveguides^{52–55}, microcavities⁶², and electrical circuits⁵⁷. However, mechanical \mathcal{PT} -symmetric systems have only been considered quite recently^{64–68}.

In our proposed mechanical \mathcal{PT} symmetric system, a lossy mechanical resonator (passive resonator) which has a weak mechanical nonlinearity is coupled to a mechanical resonator with mechanical gain (active resonator) that balances the loss of the passive resonator. The active resonator here works as a dynamical amplifier. In the vicinity of the \mathcal{PT} -phase transition, the weak nonlinearity is first distributed between the mechanically-coupled resonators and then significantly enhanced due to the localization of the mechanical supermodes in the active resonator. In this way, the effective nonlinear Kerr coefficient is increased by over three orders of magnitude. This strong nonlinearity, localized in the active resonator, blocks the phonon transport from the active resonator to the lossy resonator but permits the transport in the opposite direction.

For the experimental realization of the proposed nonlinearity-based phonon diode, we provide a system in which a mechanical beam with weak mechanical nonlinearity is coupled to another mechanical beam with gain. We show that this micro-scale system can be switched from a bidirectional transport regime to a unidirectional transport regime, and vice versa, by properly adjusting the detuning between the mechanical frequency of the resonators and the frequency of the driving phononic field, or by varying the amplitude of the input phononic field.

II. PARITY-TIME (\mathcal{PT} -) SYMMETRIC MECHANICAL SYSTEM

The system we consider here consists of two mechanical resonators, one of which has mechanical loss (passive resonator) and weak nonlinearity, and the other has mechanical gain (active resonator) but no nonlinearity (see Fig. 1). The mechanical coupling between the resonators is linear and it gives rise to the mechanical supermodes b_{\pm} with complex eigenfrequencies

$$\omega_{\pm} = \Omega_{\pm} - i\Gamma_{\pm}, \quad (1)$$

given by

$$\omega_{\pm} = \Omega_0 - i\chi \pm \beta. \quad (2)$$

Here Ω_0 is the mechanical frequency of the solitary mechanical resonators (i.e., both resonators are degenerate),

$$\chi = (\Gamma_l - \Gamma_g)/2, \quad (3)$$

$$\beta = \sqrt{g_{mm}^2 - \Gamma^2}, \quad (4)$$

$$\Gamma = (\Gamma_l + \Gamma_g)/2, \quad (5)$$

where Γ_l and Γ_g denote, respectively, the damping rate of the lossy mechanical resonator and the gain rate of the active mechanical resonator, and g_{mm} is the coupling strength between the mechanical modes. When $\Gamma \leq g_{mm}$, the system is in the \mathcal{PT} -symmetric regime, and the supermodes are non-degenerate with

$$\Omega_{\pm} = \Omega_0 \pm \beta \quad (6)$$

and have the same damping rate χ (see Figs. 3a and 3b). However, when $\Gamma > g_{mm}$, the system is in the broken- \mathcal{PT} -symmetric regime, the supermodes are frequency-degenerate with $\Omega_{\pm} = \Omega_0$ (see Figs. 3a and 3b) and have different damping rates

$$\Gamma_{\pm} = \chi \mp i\beta. \quad (7)$$

At $\Gamma = g_{mm}$, the two supermodes are degenerate with the same damping rate, indicating a transition between the \mathcal{PT} -symmetric regime and the broken- \mathcal{PT} -symmetry regime. This point is generally referred to as the \mathcal{PT} -transition point. It is seen that the two supermodes will be lossless in the \mathcal{PT} -symmetric regime if the gain and loss are well-balanced, such that $\Gamma_l = \Gamma_g$.

III. ENHANCING MECHANICAL NONLINEARITY BY BREAKING \mathcal{PT} -SYMMETRY

Let us assume that the passive resonator is made from a nonlinear acoustic material³⁵ with a small nonlinear Kerr coefficient μ . This nonlinearity mediates a cross-Kerr interaction between the two mechanical supermodes, which leads to the effective nonlinear coefficients μ'_b and μ'_s , in the broken- and unbroken- \mathcal{PT} regimes⁶⁹:

$$\mu'_b = \mu \frac{\Gamma^2 g_{mm}^2}{(\Gamma^2 - g_{mm}^2)^2}, \quad \mu'_s = \mu \frac{g_{mm}^4}{(\Gamma^2 - g_{mm}^2)^2}. \quad (8)$$

Clearly, the effective nonlinear coefficients are significantly enhanced in the vicinity of the phase transition point $\Gamma = g_{mm}$. Moreover, if the gain and loss are well-balanced, i.e., $\Gamma_l = \Gamma_g$, the supermodes become almost lossless. This observation is one of the key contributions of this paper. Namely, operating the system of two coupled mechanical resonators in the vicinity of the phase transition point will significantly enhance the existing

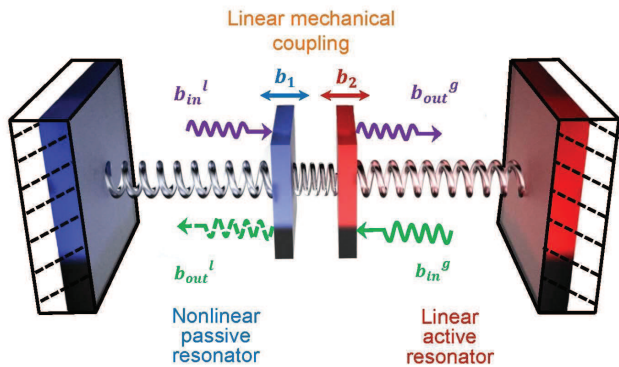


FIG. 1: (Color online) Schematic diagram of the proposed \mathcal{PT} -symmetric mechanical system. The \mathcal{PT} -symmetric mechanical system has a linear mechanical coupling between a passive mechanical resonator (having mechanical loss and very weak mechanical nonlinearity) and an active mechanical resonator (having mechanical gain but no nonlinearity). Here b_{in}^l and b_{in}^g are the input fields to the passive and active resonators, respectively, and b_{out}^l and b_{out}^g are the output fields, respectively, leaving the passive and active resonators. b_1 and b_2 denote the movable resonators.

very weak nonlinearity with an extremely small loss rate.

Using the parameter values of $\mu/\Omega_0 = 10^{-5}$, $\Gamma_l/\Omega_0 = 0.55 \times 10^{-3}$, and $\Gamma_g/\Omega_0 = 0.45 \times 10^{-3}$, we show in Fig. 3 the evolution of the eigenfrequencies of the system and of the nonlinear coefficient as a function of g_{mm}/Γ . The transition from the broken- to the unbroken- \mathcal{PT} symmetric regime and vice versa, as the mechanical coupling strength is varied, is seen in Fig. 3a and 3b and it is reflected in the bifurcations of the supermode frequencies and damping rates. Moreover, the enhancement of the nonlinearity in the vicinity of the \mathcal{PT} -phase transition point is seen in Fig. 3c. We find that the nonlinear coefficient is enhanced by more than three orders of magnitude in the vicinity of the transition point.

More interestingly, in the broken- \mathcal{PT} regime, the mechanical energy of the coupled system is localized in the active resonator, which leads to a nonlinear mechanical mode with strong self-Kerr nonlinearity localized in the active mechanical resonator. This can be interpreted intuitively as follows. The initial weak mechanical nonlinearity is transferred from the passive resonator to the active resonator and it is enhanced by field localization in the broken- \mathcal{PT} regime. Owing to the presence of the mechanical gain, the active resonator then enjoys an almost lossless mechanical mode with a giant nonlinearity (see Fig. 2).

Finally, we would like to consider how the mechanical nonlinearity will affect the \mathcal{PT} -symmetric structure of the system. Generally speaking, a strong nonlinearity will shift the transition point of a \mathcal{PT} -symmetric system or even destroy the \mathcal{PT} symmetry of such a system⁷⁰. However, in our case, we start from a system in which a

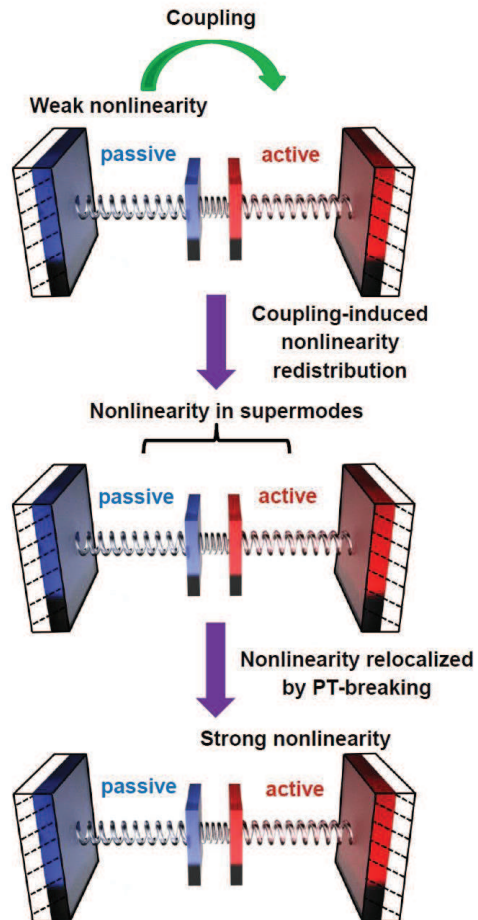


FIG. 2: (Color online) Enhancement of mechanical nonlinearity in a \mathcal{PT} -symmetric mechanical system. The coupling between two mechanical resonators creates two mechanical supermodes symmetrically distributed between the resonators, and hence both supermodes experience the weak nonlinearity of the passive resonator. In the vicinity of the \mathcal{PT} -phase transition, which takes place when the coupling strength between the resonators equals to the total loss in the system, the mechanical nonlinearity is significantly enhanced due to localization of the mechanical supermodes in the active mechanical resonator.

gain resonator is coupled to a lossy resonator with very weak Kerr nonlinearity, and thus we can omit the shift of the \mathcal{PT} -transition point induced by such a weak nonlinearity. Although we generate a strong nonlinearity in the vicinity of the \mathcal{PT} -transition point, this is an effective nonlinearity induced in the supermode picture and thus will not affect the supermodes and the \mathcal{PT} -transition point of the system.

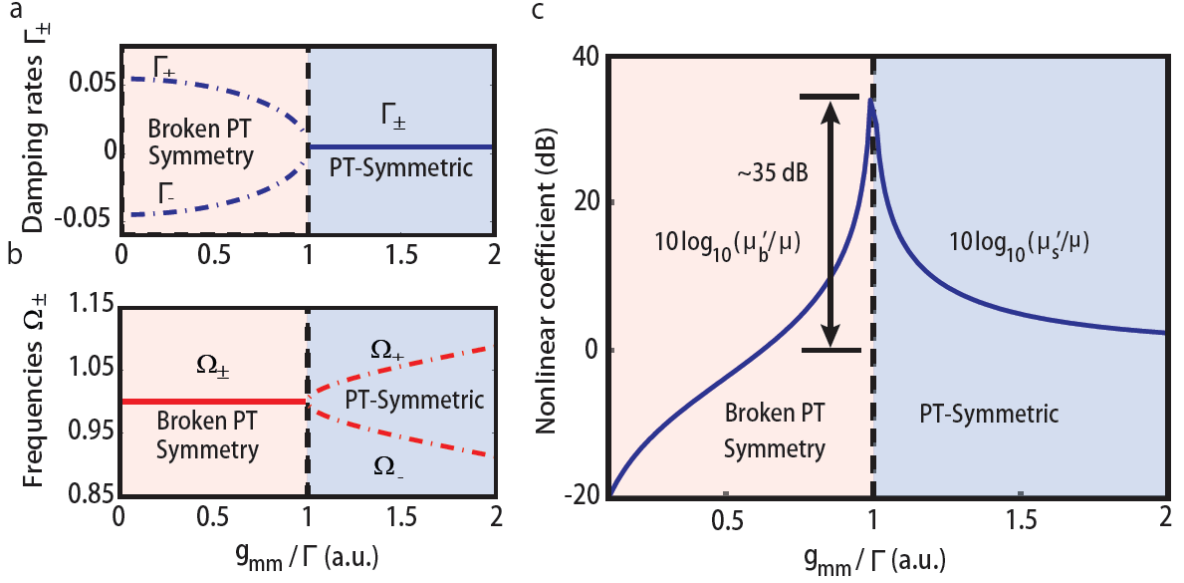


FIG. 3: (Color online) Amplification of mechanical nonlinearity via \mathcal{PT} -symmetry breaking. (a) Effective damping rates and (b) frequencies of the mechanical supermodes as functions of the normalized mechanical coupling strength g_{mm}/Γ . (c) The effective nonlinear coefficients μ'_b in the \mathcal{PT} -breaking regime and μ'_s in the \mathcal{PT} -symmetric regime. The \mathcal{PT} -phase transition takes place at $g_{mm} = \Gamma$. In the vicinity of this transition point, the nonlinear coefficients μ'_b and μ'_s are enhanced by more than three orders of magnitude (more than 35 dB increase compared to the baseline).

IV. UNIDIRECTIONAL PHONON TRANSPORT

Here we investigate the effect of the enhanced mechanical nonlinearity on the phonon transport in the coupled system. We find that the localized strong mechanical nonlinearity leads to unidirectional phonon transport from the passive resonator to the active resonator and blocks phonon transport in the opposite direction (i.e., phonon transport from the active to the passive resonator is prevented). The transport is almost lossless due to the gain-loss balance of the system. When this system is operated in the vicinity of the \mathcal{PT} -phase transition point, the unidirectional phonon transport is possible within a region given by⁶⁹

$$\delta \in \left[\frac{g_{mm}^2 \Omega_0}{\Omega_0^2 + \chi^2}, \frac{g_{mm}^2}{\Omega_0 - \sqrt{3}\chi} \right], \quad (9)$$

where

$$\delta = \Omega_0 - \Omega_d \quad (10)$$

is the detuning between the input (driving) field frequency Ω_d and the resonance frequency Ω_0 of the mechanical resonators. Additionally, in order to observe the unidirectional phonon transport, the amplitude of the input field should satisfy

$$|\varepsilon_d|^2 \in \left[\frac{2(\delta^2 + g_{mm}^2)^3}{9\mu'_b \delta^3}, \frac{2(\delta^2 + g_{mm}^2)^3}{9\mu'_b g_{mm}^2 \delta} \right], \quad (11)$$

implying that the intensity of the input field required for unidirectional transport is inversely proportional to the strength of the mechanical nonlinearity μ'_b . Since the strength of the mechanical nonlinearity can be enhanced by more than three orders of magnitude by breaking the \mathcal{PT} symmetry, the threshold of the input-field intensity for observing unidirectional phonon transport can be decreased by at least three orders of magnitude, allowing a low-threshold phonon diode operation.

To show unidirectional phonon transport in the broken- \mathcal{PT} regime, let us first fix the amplitude of the input field and vary the detuning δ . We compare the amplitude transmittance

$$t_{l \rightarrow g} = b_{\text{out}}^g / b_{\text{in}}^l \quad (12)$$

and

$$t_{g \rightarrow l} = b_{\text{out}}^l / b_{\text{in}}^g. \quad (13)$$

The former, $t_{l \rightarrow g}$, denotes the transmission from the passive to the active resonator, that is, the system is driven by a phononic input field b_{in}^l of frequency Ω_d at the passive resonator side and the output b_{out}^g is measured at the active resonator side. However, the latter, $t_{g \rightarrow l}$, denotes the amplitude transmittance from the active resonator to the passive resonator when the system is driven by the field b_{in}^g of frequency Ω_d at the active resonator side and the output b_{out}^l is measured at the passive side. The nonlinearity in the system manifests as a bistability and hysteresis in the power transmittance,

$$T_{g \rightarrow l} = |t_{g \rightarrow l}|^2 \quad (14)$$

and

$$T_{l \rightarrow g} = |t_{l \rightarrow g}|^2, \quad (15)$$

obtained as the detuning δ is up-scanned from smaller to larger detuning and down-scanned from larger to smaller detuning (see Fig. 4a).

We find that during the down-scan, both of the transmittances $T_{l \rightarrow g}$ and $T_{g \rightarrow l}$ stay at the lower branch with values close to zero until $\delta/\Omega_0 = 0.5 \times 10^{-3}$, after which they bifurcate from each other only slightly and then jump to the stable points at the upper branch of their respective trajectories (see Fig. 4a). Further decreasing the detuning leads to an increase in $T_{l \rightarrow g}$, but a decrease in $T_{g \rightarrow l}$. This implies that there is no unidirectional phonon transport with the parameter values used in the numerical simulations. Instead, when the detuning is below a critical value, the phonon transport is bidirectional; whereas when it is above that critical value there is no phonon transport.

During the up-scan, however, after a short stay on the stable state, i.e., a regime in which there is no bistability and hysteresis in the transmittance, (during which $T_{l \rightarrow g}$ decreases and $T_{g \rightarrow l}$ increases with growing detuning), both of the transmittances follow the upper branches of their trajectories, during which a linear increase in $T_{g \rightarrow l}$ and a slow-rate decrease in $T_{l \rightarrow g}$ are observed (see Fig. 4a). This behavior continues until $\delta/\Omega_0 \sim 2.5 \times 10^{-3}$ for $T_{g \rightarrow l}$, where it jumps to the lower branch of its trajectory, and becomes zero as the detuning is increased (see Fig. 4a). This implies that phonon transport from the active mechanical resonator to the passive one is prevented if the detuning is set to $\delta/\Omega_0 > 2.5 \times 10^{-3}$. The transmittance $T_{l \rightarrow g}$ stays at its upper branch with a value close to one until $\delta/\Omega_0 \sim 3 \times 10^{-3}$, where it jumps to its lower branch and becomes zero. Thus, for $\delta/\Omega_0 > 3 \times 10^{-3}$, phonon transport from the passive to the active resonator is prevented. Clearly, in the detuning region $2.5 \times 10^{-3} < \delta/\Omega_0 < 3 \times 10^{-3}$, the transmittance $T_{l \rightarrow g}$ is close to one whereas $T_{g \rightarrow l}$ is close to zero in this detuning region phonon transport from the active mechanical resonator to the passive one is forbidden, whereas phonon transport from the passive mechanical resonator to active one is allowed with almost no loss. Thus, we conclude that phonon transmission is non-reciprocal in this detuning region, and the rectification is ~ 30 dB within the nonreciprocal transport region (see Fig. 4a). For detuning values smaller than the lower bound of this region, phonon transport is bidirectional. For detuning values larger than the upper bound of the region, phonon transport is not possible.

Note that our phonon diode should work only when the disturbance and perturbation of the system parameters are not too strong. In fact, within the unidirectional phonon transport window shown in Fig. 4a, the transmittance $T_{l \rightarrow g}$ has two different branches of metastable values. When we increase the detuning δ within this unidirectional phonon transport window, $T_{l \rightarrow g}$ will stay in the upper stable branch if we do not severely disturb the

system and the phonon diode should operate properly. However, if the disturbance is too strong, $T_{l \rightarrow g}$ will jump from the upper branch to the lower branch and stay in this stable lower branch, without rectification.

Alternatively, we can fix the detuning and vary the amplitude of the input field to show the nonlinearity-induced bistability and hysteresis. A nonreciprocal phonon transport region is seen when the amplitude of the input field is up-scanned (see Fig. 4b). The nonreciprocal transport region disappears when the amplitude of the input field is down-scanned. Within the nonreciprocal transport region, when the input is varied at fixed detuning (see Fig. 4b), the rectification is ~ 30 dB. Similarly, in this case, due to the metastability of the transmittance $T_{l \rightarrow g}$, the disturbance-induced perturbation of the system parameters may not be too strong otherwise our design of phonon diode will be invalid.

V. ON-CHIP PHONON DIODE

The unidirectional phonon transport enabled by the \mathcal{PT} -breaking-induced strong mechanical nonlinearity can be used to fabricate lossless phonon diodes in on-chip systems. This may have many applications, such as single-phonon transistors and routers, on-chip quantum switches, and information-processing components. One possible way to realize the proposed phonon diode is to use coupled beams and cantilevers (see Fig. 5a). Phonon lasing, and hence an active mechanical resonator, has been experimentally realized in an electromechanical beam⁷¹. Elastically-coupled nano beams and cantilevers, by which the mechanical supermodes can be generated, have also been shown in various experiments⁷²⁻⁷⁵, in which the two mechanical resonators can be independently driven⁷³. Thus our proposal is within the reach of current experimental techniques of nano-micro-electromechanical systems.

Let us now consider the design of the phonon diode system shown in Fig. 5 in which a lossy vibrating beam with damping rate Γ_l and a weak Kerr nonlinearity³⁵ of strength μ is elastically coupled to another vibrating beam with gain Γ_g ⁷¹. The frequencies of the two beams are both Ω_0 and the mechanical coupling strength is g_{mm} .

In Fig. 6, we present the numerical results performed with the system parameters: $\Omega_0 = 600$ kHz, $\Gamma_l = 33$ kHz, $\Gamma_g = 30$ kHz, $\delta = 1.65$ kHz, $\mu = 5.7$ kHz, and $g_{mm} = 1$ kHz. Here, we fix the detuning δ and change the amplitude of the input field. There is a 50 dB background noise which includes the combined effect of the thermal noise on the mechanical resonators, the electrical noises induced by the measurement apparatus and other possible sources of noise. The results shown in Fig. 6 for the phonon diode agree well with the general model discussed in the previous section. When the amplitude of the input field is increased, it is clearly seen that there is a nonreciprocal region in which phonon transport

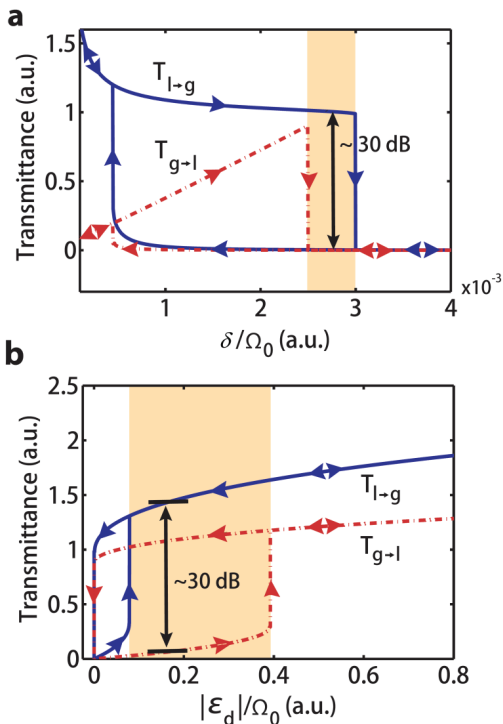


FIG. 4: (Color online) Unidirectional phonon transport by \mathcal{PT} -symmetry breaking. (a) Unidirectional phonon transport when the detuning δ is varied. The transmittance from the active to passive mechanical resonator $T_{g \rightarrow l}$ (red dash-dotted curve), and from the passive to the active mechanical resonator $T_{l \rightarrow g}$ (blue solid curve) versus the detuning $\delta = \Omega_0 - \Omega_d$ shows a strong bistability and hysteresis effect. The transmittance functions evolve along different trajectories for increasing and decreasing detuning due to the nonlinearity-induced bistability. A unidirectional phonon-transport region (melon-colored shaded region) appears only when the detuning δ is up-scanned from smaller to larger detunings. Within this regime, the rectification is ~ 30 dB. (b) Unidirectional phonon transport when the amplitude of the input field is varied at fixed detuning $\delta/\Omega_0 = 2.75 \times 10^{-3}$. Within the unidirectional transport region (melon-colored shaded region), rectification is ~ 30 dB.

from the active beam to the passive beam is almost completely suppressed (see Fig. 6b(ii)), but phonon transport from the passive beam to the active beam is allowed (see Fig. 6a(ii)). A rectification ratio of about 30 dB is obtained. When the amplitude of the phonon excitation is larger than the upper bound of the unidirectional phonon transport region, the transport is bidirectional. In this case, the phonons can freely move from the active beam to the passive beam and vice versa (see Figs. 6a(i) and 6b(i)). Finally, for amplitudes of the phonon excitation smaller than the lower bound of the region, no phonon transport can take place between the resonators (see Figs. 6a(iii) and 6b(iii)). These are the result of hysteresis (see Fig. 4b) caused by the strong mechanical nonlinearity.

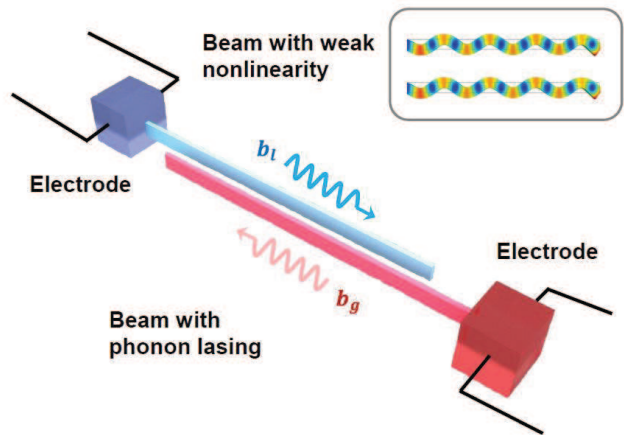


FIG. 5: (Color online) Schematic diagram of the phonon diode system with two mechanical beams in which a beam with weak mechanical nonlinearity is electrically or elastically coupled to another beam with mechanical gain. The insets show the finite-element-method (FEM) simulation by Comsol for the mechanical modes.

VI. DISCUSSIONS

We have proposed a method to generate ultra-strong mechanical nonlinearity with a very low-loss rate using a \mathcal{PT} -symmetric mechanical structure in which a mechanical resonator with gain but no nonlinearity is coupled to a lossy (i.e., passive mechanical loss and no gain) mechanical resonator with very weak nonlinearity. We have showed that the weak mechanical nonlinearity is redistributed in the supermodes of the coupled mechanical system and is enhanced (by more than three orders of magnitude) when the mechanical \mathcal{PT} system enters the broken- \mathcal{PT} regime. Moreover, owing to the presence of the mechanical gain in one of the resonators to compensate the mechanical loss of the other resonator, the effective mechanical damping rate is decreased in the \mathcal{PT} -symmetric system. Using experimentally accessible parameter values, we identified the regimes where unidirectional phonon transport is possible from the passive to active resonator but not in the opposite direction. We then proposed an experimentally-realizable system where a mechanical beam with passive loss and weak nonlinearity is coupled to another beam which acts like an active mechanical resonator. A possible bottleneck for this design to achieve a phonon diode operated in ambient condition is whether the mechanical gain observed with the mechanical beams in a controlled environment and at low temperatures³⁶ could also be obtained in ambient-temperature conditions. A possible way to overcome this problem, and to realize phonon diodes in ambient conditions, is to use a hybrid system composed of a gain optomechanical resonator and a nonlinear electrically-driven mechanical beam³⁵, where the coupling between them is achieved via the evanescent

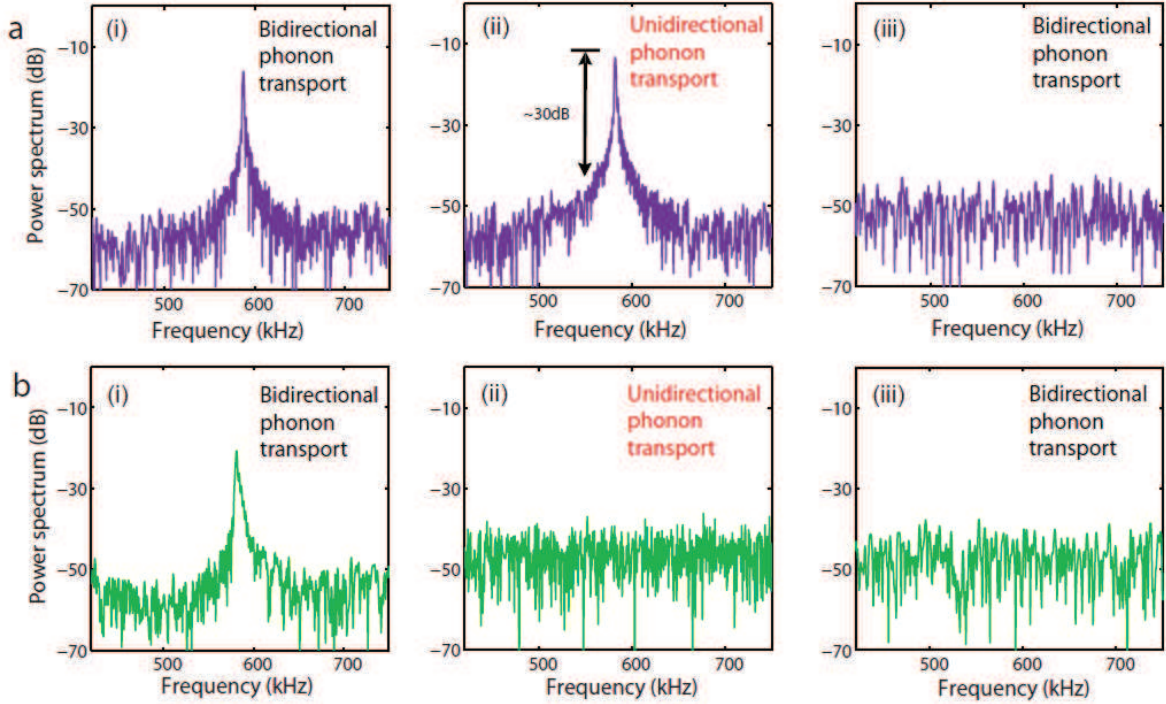


FIG. 6: (Color online) Numerical results demonstrating unidirectional phonon transport in a \mathcal{PT} -symmetric mechanical system in the broken- \mathcal{PT} phase. (a) Power spectrum obtained at the output of the active beam without mechanical nonlinearity when the phonon excitation (input) is at the passive beam with weak nonlinearity. (b) Power spectrum obtained at the output of the passive beam when the phonon excitation (input) is at the active beam. When the intensity of the phonon excitation is within the region bounded by Eq. (11), phonon transport is unidirectional. Transport from the passive to the active resonator is allowed [see a(ii)], but the transport from the active to the passive resonator is prevented [b(ii)]. The rectification is about 30 dB. If the intensity of the phonon excitation is larger than the upper bound of the unidirectional transport region, phonon transport is bidirectional [a(i) and b(i)]. Phonon transport is not allowed in either of the directions [a(iii) and b(iii)] if the intensity of the phonon excitation is smaller than the lower bound of the region given in Eq. (11).

optical field of the optomechanical resonator⁷⁶. The mechanical gain of the optomechanical resonators can be provided at ambient conditions by, e.g., the optomechanical dynamical instability in the blue detuning regime⁷⁷, which has been demonstrated in optomechanical resonators in various experiments⁷⁸. Since creating strongly-nonlinear mechanical or acoustic materials remains challenging, we believe that the proposed system and the developed approach provide a suitable platform for investigating nonlinear phononics and can be used as a building block to design more complex hybrid optomechanical or electromechanical information processors. We envision that \mathcal{PT} mechanical systems will open a new route for designing functional phononic systems with nonreciprocal phonon responses.

ACKNOWLEDGMENTS

JZ is supported by the NSFC under Grant Nos. 61174084, 61134008. YXL is supported by the NSFC under Grant Nos. 10975080, 61025022, 91321208. YXL and JZ are supported by the National Basic Research

Program of China (973 Program) under Grant No. 2014CB921401, the Tsinghua University Initiative Scientific Research Program, and the Tsinghua National Laboratory for Information Science and Technology (TNList) Cross-discipline Foundation. LY and SKO are supported by ARO grant No. W911NF-12-1-0026 and the NSFC under Grant No. 61328502. F.N. is supported by the RIKEN iTHES Project, MURI Center for Dynamic Magneto-Optics via the AFOSR award number FA9550-14-1-0040, and Grant-in-Aid for Scientific Research (A).

AUTHOR CONTRIBUTIONS

JZ, BP, SKO contributed equally to this work. LY, FN, SKO, YXL supervised the project.

Appendix A: Nonlinearity enhancement by broken \mathcal{PT} symmetry

In order to prove the enhancement of mechanical nonlinearity in the broken- \mathcal{PT} -symmetric regime, let us con-

sider a system of two coupled mechanical resonators, in which one of the resonators has mechanical gain (active resonator) and thus a positive damping rate Γ_g and the second mechanical resonator has a passive mechanical loss (passive resonator) with loss rate Γ_l . The resonators have the same mechanical frequency Ω_0 , and the annihilation operators for their mechanical modes are denoted as b_g and b_l , respectively, for the active and passive resonators. Moreover, the passive mechanical resonator has a weak mechanical Kerr-nonlinearity denoted by μ . The Hamiltonian describing these coupled mechanical resonators can be written as

$$H = (\Omega_0 - i\Gamma_l) b_l^\dagger b_l + (\Omega_0 + i\Gamma_g) b_g^\dagger b_g + g_{mm} (b_l^\dagger b_g + b_l b_g^\dagger) + \mu (b_l^\dagger b_l)^2, \quad (\text{A1})$$

where g_{mm} is the coupling strength between the mechanical modes of the resonators. Generally, the nonlinear Kerr term in Eq. (A1) will shift the boundary between the \mathcal{PT} symmetric regime and the broken- \mathcal{PT} regime. However, in our model, the Kerr nonlinearity denoted by μ is very weak, and we can omit the nonlinearity-induced shift of this boundary. To find the boundary of \mathcal{PT} transition, we consider the first three terms in Eq. (A1)

$$H_1 = (\Omega_0 - i\Gamma_l) b_l^\dagger b_l + (\Omega_0 + i\Gamma_g) b_g^\dagger b_g + g_{mm} (b_l^\dagger b_g + b_l b_g^\dagger), \quad (\text{A2})$$

which can be written as

$$H_1 = \begin{pmatrix} b_g^\dagger & b_l^\dagger \end{pmatrix} \begin{pmatrix} \Omega_0 + i\Gamma_g & g_{mm} \\ g_{mm} & \Omega_0 - i\Gamma_l \end{pmatrix} \begin{pmatrix} b_g \\ b_l \end{pmatrix}. \quad (\text{A3})$$

This Hamiltonian can be diagonalized as

$$H_1 = \begin{pmatrix} b_g^\dagger & b_l^\dagger \end{pmatrix} P^{-1} \begin{pmatrix} \Omega_+ - i\Gamma_+ & 0 \\ 0 & \Omega_- - i\Gamma_- \end{pmatrix} P \begin{pmatrix} b_g \\ b_l \end{pmatrix}, \quad (\text{A4})$$

where the transformation matrix P is defined by

$$P = \frac{\begin{pmatrix} g_{mm} [(\Omega_+ - \Omega_0) - i(\Gamma_+ - \Gamma_l)] \\ g_{mm} [(\Omega_- - \Omega_0) - i(\Gamma_- - \Gamma_l)] \end{pmatrix}}{\sqrt{(\Omega_\pm - \Omega_0)^2 + (\Gamma_\pm - \Gamma_l)^2 + g_{mm}^2}}. \quad (\text{A5})$$

Consequently, we have

$$\begin{pmatrix} b_+ \\ b_- \end{pmatrix} = P \begin{pmatrix} b_g \\ b_l \end{pmatrix} \quad (\text{A6})$$

as the mechanical supermodes formed by the coupling of the resonators. These supermodes b_\pm are characterized by the eigenfrequencies Ω_\pm and damping rates Γ_\pm .

For this mechanical \mathcal{PT} symmetric system, there are two different regimes (see Fig. 7):

(i) \mathcal{PT} symmetric regime where

$$\Gamma = \frac{(\Gamma_l + \Gamma_g)}{2} \leq g_{mm}, \quad (\text{A7})$$

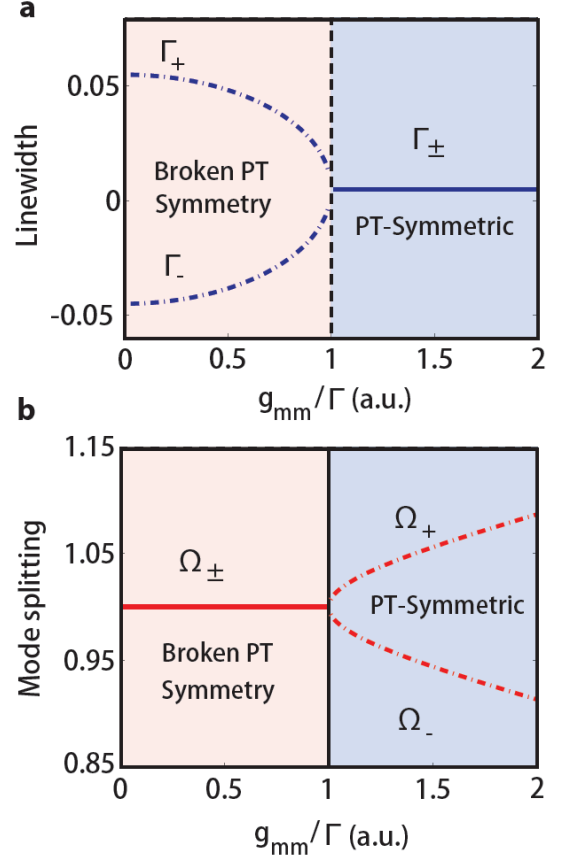


FIG. 7: (Color online). Evolution of the eigenfrequencies of the coupled mechanical resonators. (a) Difference of the real parts of the eigenfrequencies of the supermodes: mode splitting, and (b) difference of the imaginary parts of the eigenfrequencies (i.e., linewidth) of the supermodes. The resonance frequencies of the supermodes are non-degenerate in the \mathcal{PT} -symmetric regime. In the broken- \mathcal{PT} symmetry regime, however, they are frequency degenerate.

and the two supermodes b_+ and b_- are nondegenerate in their resonance frequencies (i.e., real part of their complex eigenfrequencies) given by

$$\Omega_\pm = \Omega_0 \pm \beta = \Omega_0 \pm \sqrt{g_{mm}^2 - \Gamma^2}. \quad (\text{A8})$$

The damping rates of the supermodes (i.e., linewidths of the resonances; imaginary part of their complex eigenfrequencies) are the same and equal to

$$\Gamma_\pm = \chi = \frac{\Gamma_l - \Gamma_g}{2}. \quad (\text{A9})$$

(ii) Broken \mathcal{PT} -symmetry regime where

$$\Gamma = \frac{\Gamma_l + \Gamma_g}{2} > g_{mm}. \quad (\text{A10})$$

The two supermodes b_+ and b_- are degenerate in their resonance frequencies

$$\Omega_\pm = \Omega_0, \quad (\text{A11})$$

and their damping rates are different:

$$\Gamma_{\pm} = \chi \mp i\beta. \quad (\text{A12})$$

Now let us consider the nonlinear Kerr term in Eq. (A1). Using Eq. (A6), we find

$$\begin{aligned} b_l &= \frac{\sqrt{(\Omega_+ - \Omega_0)^2 + (\Gamma_+ - \Gamma_l)^2 + g_{mm}^2}}{(\Omega_+ - \Omega_-) - i(\Gamma_+ - \Gamma_-)} b_+ \\ &\quad - \frac{\sqrt{(\Omega_- - \Omega_0)^2 + (\Gamma_- - \Gamma_l)^2 + g_{mm}^2}}{(\Omega_+ - \Omega_-) - i(\Gamma_+ - \Gamma_-)} b_- \\ &= \beta_{l+} b_+ + \beta_{l-} b_-. \end{aligned}$$

By substituting the above equation into the last term on the right hand side of Eq. (A1) and dropping the non-resonant terms, we can rewrite the nonlinear Kerr term of Eq. (A1) as

$$H_{nl} = \left(|\beta_{l+}|^2 b_+^\dagger b_+ + |\beta_{l-}|^2 b_-^\dagger b_- \right)^2. \quad (\text{A13})$$

The self-Kerr terms $|\beta_{l+}|^4 (b_+^\dagger b_+)^2$ and $|\beta_{l-}|^4 (b_-^\dagger b_-)^2$ only lead to a frequency-shift of the two supermodes and thus are less important. The cross-Kerr term

$$H'_{nl} = |\beta_{l+}|^2 |\beta_{l-}|^2 (b_+^\dagger b_+) (b_-^\dagger b_-) = \mu' (b_+^\dagger b_+) (b_-^\dagger b_-) \quad (\text{A14})$$

is more important and leads to the redistribution of the nonlinear effect among the two supermodes. From Eqs. (A7)-(A9), the nonlinear coefficient $2|\beta_{l+}|^2 |\beta_{l-}|^2$ can be represented in the broken- \mathcal{PT} regime as μ'_b , and in the \mathcal{PT} symmetric regime as μ'_s

$$\mu'_b = \mu \frac{\Gamma^2 g_{mm}^2}{(\Gamma^2 - g_{mm}^2)^2}, \quad \mu'_s = \mu \frac{g_{mm}^4}{(\Gamma^2 - g_{mm}^2)^2}. \quad (\text{A15})$$

As was observed in photonic experiments^{62,79}, in the broken- \mathcal{PT} regime the two supermodes b_{\pm} are degenerate and the field is localized in the gain resonator, and thus the field b_l is much smaller than b_g . Therefore, we can omit the terms related to b_l in the expressions of the supermodes b_{\pm} and we have

$$\begin{aligned} b_+ &\approx \frac{g_{mm}}{\sqrt{(\Omega_+ - \Omega_0)^2 + (\Gamma_+ - \Gamma_l)^2 + g_{mm}^2}} b_g, \\ b_- &\approx \frac{g_{mm}}{\sqrt{(\Omega_- - \Omega_0)^2 + (\Gamma_- - \Gamma_l)^2 + g_{mm}^2}} b_g. \end{aligned}$$

Subsequently, we find that the cross-Kerr term given in Eq. (A14) can induce a self-Kerr effect in the gain resonator

$$H'_{nl} = \mu \frac{g_{mm}^4}{4(\Gamma^2 - g_{mm}^2)^2} (b_g^\dagger b_g)^2. \quad (\text{A16})$$

Clearly, when $\Gamma \approx g_{mm}$ (in the vicinity of the spontaneous \mathcal{PT} -symmetry breaking point: the \mathcal{PT} -phase

transition point), this self-Kerr nonlinearity is greatly enhanced.

Appendix B: Unidirectional phonon transport by mechanical nonlinearity

Let us now present a detailed analysis for finding the unidirectional phonon transport region near the \mathcal{PT} -transition point. In this case, the gain-loss balance between the active resonator, with annihilation operator b_l , and the passive resonator, with annihilation operator b_r , decreases the effective damping rates of the two modes. In the vicinity of the \mathcal{PT} -phase transition point (i.e., $\Gamma \approx g_{mm}$), the effective damping rates of the two modes is given by $\chi = (\Gamma_l - \Gamma_g)/2$. The coupling between the two mechanical resonators also leads to the transfer of mechanical Kerr nonlinearity from the passive resonator to the active resonator, and this mechanical nonlinearity is strongly enhanced near the \mathcal{PT} -transition point (i.e., $\Gamma \approx g_{mm}$). Hereafter, we will denote this enhanced mechanical Kerr nonlinearity coefficient as μ'_b .

Let us first consider the phonon transport from the passive resonator to the active resonator. Here the phononic field in the passive resonator is generated via an phononic input field with strength ε_d and frequency Ω_d . Using the standard input-output formalism^{80,81}, the output field of the active mechanical resonator is found as $b_{\text{out}} = \chi^{1/2} b_g$, which shows that the output field is proportional to the intracavity field b_g , if we omit the vacuum fluctuations in the input field. Thus the transmission from passive to active resonator is given by

$$T_{l \rightarrow g}(\delta) = \chi n_g / |\varepsilon_d|^2, \quad (\text{B1})$$

where n_g represents the steady-state value of the intracavity phonon number in the active resonator. From the steady-state solution of the equations of motion for the coupled mechanical resonator system, we find that n_g satisfies

$$\tilde{\mu}^2 n_g^3 - 2\tilde{\mu} \tilde{\Omega} n_g^2 + (\tilde{\Gamma}^2 + \tilde{\Omega}^2) n_g - \tilde{n}_{\text{in}} = 0, \quad (\text{B2})$$

where

$$\begin{aligned} \tilde{\Gamma} &= (\chi^2 + \delta^2 + g_{mm}^2) \chi, \quad \tilde{\Omega} = (\chi^2 + \delta^2) \Omega_0 - g_{mm}^2 \delta, \\ \tilde{\mu} &= (\chi^2 + \delta^2) \mu'_b, \quad \tilde{n}_{\text{in}} = |\varepsilon_d|^2 g_{mm}^2 (\chi^2 + \delta^2). \end{aligned}$$

The algebraic equation (B2) has three or one root depending on the system parameters, and one of the roots is unstable if the algebraic equation (B2) has three roots. When we increase the detuning $\delta = \Omega_0 - \Omega_d$, such that

$$\frac{\Omega_0 - (g_{mm}^2 \delta) / (\chi^2 + \delta^2)}{\chi (\chi^2 + \delta^2 + g_{mm}^2) / (\chi^2 + \delta^2)} = \sqrt{3}, \quad (\text{B3})$$

or equivalently,

$$\delta = \delta_{\max} = \frac{g_{mm}^2 + \sqrt{g_{mm}^4 + 4(\sqrt{3}\chi^3 - \chi^2\Omega_0 + \sqrt{3}g_{mm}^2\chi)(\Omega_0 - \sqrt{3}\chi)}}{2(\Omega_0 - \sqrt{3}\chi)}, \quad (\text{B4})$$

the system enters the bistable regime. In fact, when $\delta \leq \delta_{\max}$, the algebraic equation has three branches of solutions. However, two branches of solutions disappear when $\delta > \delta_{\min}$ (see Ref.⁸² and the supplementary materials of Ref.⁸³). In this case, the transmittance of the photon transport $T_{l \rightarrow g}(\delta)$ changes suddenly from a high value to a low value. Noting that $g_{mm} \gg \chi$ near the \mathcal{PT} breaking point, the critical detuning δ_{\max} can be approximately estimated to be

$$\delta_{\max} = \frac{g_{mm}^2}{\Omega_0 - \sqrt{3}\chi}. \quad (\text{B5})$$

Let us now consider the phonon transport from the active mechanical resonator to the passive one. The driving field with strength ε_d and frequency Ω_d is fed into the gain resonator in this case. Following the same discussion and approach as for the previous case, it can be shown that a bistability-induced phase transition occurs when the detuning $\delta = \Omega_0 - \Omega_d$ satisfies

$$\frac{\delta - (g_{mm}^2\Omega_0) / (\chi^2 + \Omega_0^2)}{\chi(\chi^2 + \Omega_0^2 + g_{mm}^2) / (\chi^2 + \Omega_0^2)} = \sqrt{3}, \quad (\text{B6})$$

or equivalently,

$$\delta = \delta_{\min} = \frac{\sqrt{3}(\chi^2 + \Omega_0^2 + g_{mm}^2)\chi + g_{mm}^2\Omega_0}{\chi^2 + \Omega_0^2}. \quad (\text{B7})$$

Near the \mathcal{PT} -breaking point, $\chi \ll g_{mm}, \Omega_0$, and thus δ_{\min} can be approximately estimated to be

$$\delta_{\min} = \frac{g_{mm}^2\Omega_0}{\chi^2 + \Omega_0^2}. \quad (\text{B8})$$

Combing Eqs. (B5) and (B8), we find that when the detuning δ is within the following region

$$[\delta_{\min}, \delta_{\max}] = \left[\frac{g_{mm}^2\Omega_0}{\Omega_0^2 + \chi^2}, \frac{g_{mm}^2}{\Omega_0 - \sqrt{3}\chi} \right], \quad (\text{B9})$$

it is possible to observe the unidirectional phonon transport, i.e., the phonon transport from the passive resonator to the active resonator is allowed, whereas the phonon transport from the active resonator to the passive resonator is blocked.

Figure. 8a shows the transmittance functions $T_{l \rightarrow g}(\delta)$ and $T_{g \rightarrow l}(\delta)$ as a function of the detuning δ . It is (as explained in the main text) clear that there is a unidirectional phonon transport region when the detuning is up-scanned from smaller to larger detuning. We also show in Fig. 8b the rectification ratios for up-scanning and down-scanning the detuning δ . Similar to our previous discussions, a non-reciprocal region can be observed for the up-scanning process, while it disappears for the down-scanning process, and a high rectification-ratio, larger than 30 dB, can be obtained within the nonreciprocal region.

Up to this point, we do not consider the amplitude of the input field. Let us assume that the detuning δ is fixed and is within the detuning region given by Eq. (B9). We then vary the amplitude of the input field to show the bistability and the hysteresis in the transmittance functions. Let us first assume that $\delta > g_{mm}$. If we consider the phonon transport from the passive resonator to the active resonator, we can obtain an algebraic equation similar to that given in Eq. (B2). The bistable transition point corresponds to the stationary points of the function

$$f(n_g) = \tilde{\mu}^2 n_g^3 - 2\tilde{\mu}\tilde{\Omega} n_g^2 + (\tilde{\Gamma}^2 + \tilde{\Omega}^2) n_g. \quad (\text{B10})$$

By setting $f'(n_g) = 0$, the stationary point of $f(n_g)$ can be found as

$$n_g^* = \left[2\tilde{\mu}\tilde{\Omega} - \sqrt{4\tilde{\mu}^2\tilde{\Omega}^2 - 3\tilde{\mu}^2(\tilde{\Gamma}^2 + \tilde{\Omega}^2)} \right] (3\tilde{\mu}^2)^{-1}. \quad (\text{B11})$$

The upper bound of the unidirectional phonon transport region is given by

$$|\varepsilon_{\max}|^2 = \frac{f(n_g^*)}{g_{mm}^2(\chi^2 + \delta^2)} = \frac{2\tilde{\Omega}(\tilde{\Gamma}^2 + \tilde{\Omega}^2)}{9\tilde{\mu}g_{mm}^2(\chi^2 + \delta^2)} + \frac{(6\tilde{\Gamma}^2 - 2\tilde{\Omega}^2)}{9g_{mm}^2(\chi^2 + \delta^2)} \left[\frac{2\tilde{\mu}\tilde{\Omega} - \sqrt{4\tilde{\mu}^2\tilde{\Omega}^2 - 3\tilde{\mu}^2(\tilde{\Gamma}^2 + \tilde{\Omega}^2)}}{3\tilde{\mu}^2} \right].$$

Near the \mathcal{PT} -transition point, we have $\delta, g_{mm} \gg \chi$, and

thus it can be approximately estimated that

$$|\varepsilon_{\max}|^2 \approx \frac{2(\delta^2 + g_{mm}^2)^2}{9\mu_b' g_{mm}^2 \delta}. \quad (\text{B12})$$

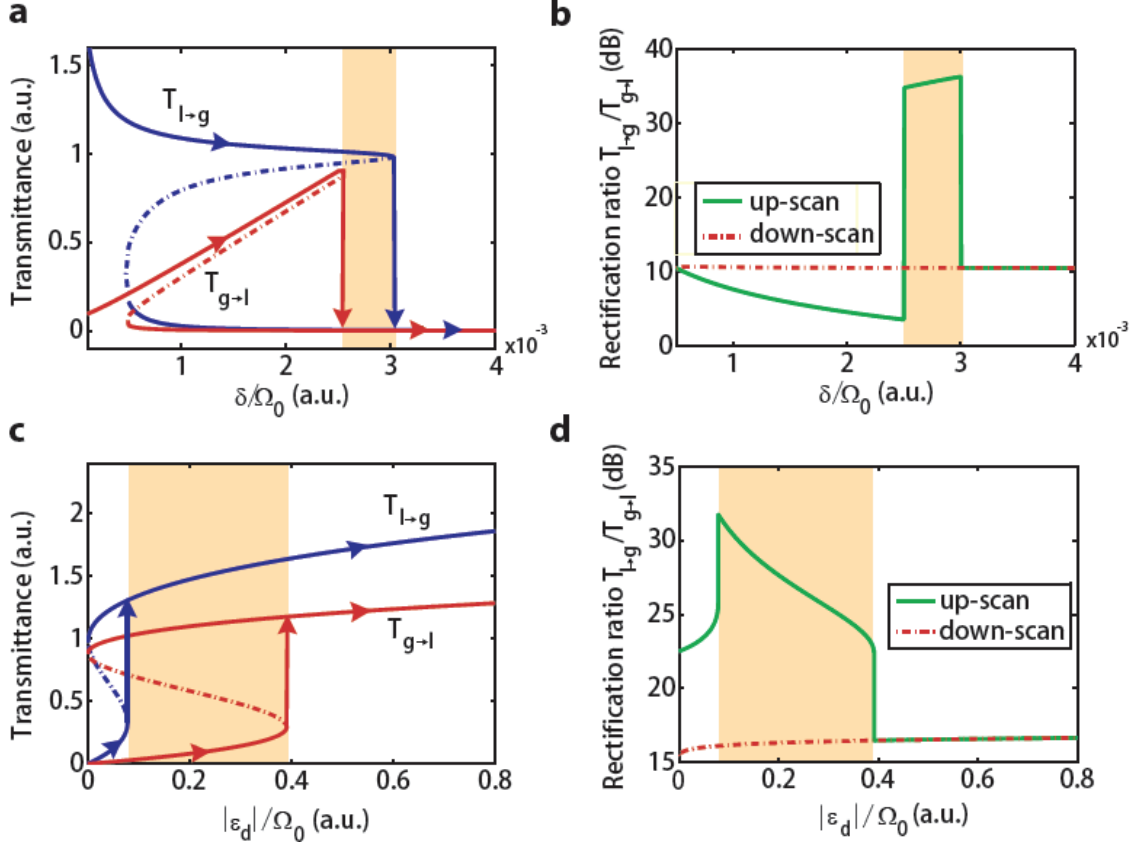


FIG. 8: (Color online). Bistability curves and unidirectional phonon-transport regions. (a) Transmittances as a function of the detuning frequency δ , when the input field amplitude is fixed at ε_d . (b) Rectification ratio for the bidirectional phonon transport versus the detuning δ : a rectification ratio larger than 30 dB can be obtained when the detuning is up-scanned to enter the unidirectional phonon transport region. (c) Transmittances as function of the intensity of the input field when the detuning frequency δ is fixed and its value is taken within the unidirectional phonon transport region in (a). The blue and red curves represent the power transmittances from the passive to the active resonator $T_{l \rightarrow g}$ and from the active to the passive resonator $T_{g \rightarrow l}$. The solid and dashed parts on each curve denote the stable and unstable solutions of the bistable system. The unstable solutions cannot be observed in the output and thus lead to sudden transitions (black solid arrows) in the transmittance functions. (d) Rectification ratios versus normalized amplitude of the input field for fixed detuning δ . The melon-colored shaded areas denote the unidirectional transport regions.

Let us now consider the case of phonon transport from the active resonator to the passive resonator when the amplitude of the input field is varied and the detuning is kept fixed. In this case, we obtain

$$\tilde{\mu}^2 n_g^3 - 2\tilde{\mu}\tilde{\Omega}n_g^2 + (\tilde{\Gamma}^2 + \tilde{\Omega}^2)n_g - \tilde{n}_{\text{in}} = 0, \quad (\text{B13})$$

where

$$\begin{aligned} \tilde{\Gamma} &= (\chi^2 + \Omega_0^2 + g_{mm}^2)\chi, & \tilde{\Omega} &= (\chi^2 + \Omega^2)\delta - g_{mm}^2\Omega_0, \\ \tilde{\mu} &= (\chi^2 + \Omega_0^2)\mu'_b, & \tilde{n}_{\text{in}} &= (\chi^2 + \delta^2)^2|\varepsilon_d|^2. \end{aligned}$$

Similar to Eq. (B10), the bistable transition point can be found by calculating the stationary points of the function

$$f(n_g) = \tilde{\mu}^2 n_g^3 - 2\tilde{\mu}\tilde{\Omega}n_g^2 + (\tilde{\Gamma}^2 + \tilde{\Omega}^2)n_g. \quad (\text{B14})$$

which leads to

$$\tilde{n}_g^* = \left[2\tilde{\mu}\tilde{\Omega} - \sqrt{4\tilde{\mu}^2\tilde{\Omega}^2 - 3\tilde{\mu}^2(\tilde{\Gamma}^2 + \tilde{\Omega}^2)} \right] (3\tilde{\mu}^2)^{-1}. \quad (\text{B15})$$

The lower bound of the unidirectional phonon transport region is then given by

$$|\varepsilon_{\text{min}}|^2 = \frac{f(\tilde{n}_g^*)}{(\chi^2 + \delta^2)^2} = \frac{2\tilde{\Omega}(\tilde{\Gamma}^2 + \tilde{\Omega}^2)}{9\tilde{\mu}(\chi^2 + \delta^2)^2} + \frac{(6\tilde{\Gamma}^2 - 2\tilde{\Omega}^2)}{9g_{mm}^2(\chi^2 + \delta^2)} \left[\frac{2\tilde{\mu}\tilde{\Omega} - \sqrt{4\tilde{\mu}^2\tilde{\Omega}^2 - 3\tilde{\mu}^2(\tilde{\Gamma}^2 + \tilde{\Omega}^2)}}{3\tilde{\mu}^2} \right].$$

Near the \mathcal{PT} -transition point, we have $\delta, g_{mm} \gg \chi$, and

it can be approximately estimated that

$$|\varepsilon_{\min}|^2 \approx \frac{2(\delta^2 + g_{mm}^2)^2}{9\mu'_b \delta^3}. \quad (\text{B16})$$

We thus conclude that nonreciprocal phonon transport takes place if the amplitude of the input is within the region

$$|\varepsilon_d|^2 \in \left[\frac{2(\delta^2 + g_{mm}^2)^3}{9\mu'_b \delta^3}, \frac{2(\delta^2 + g_{mm}^2)^3}{9\mu'_b g_{mm}^2 \delta} \right]. \quad (\text{B17})$$

Similarly, when $\delta \leq g_{mm}$, the nonreciprocal region for the amplitude of the input field can be written as

$$|\varepsilon_d|^2 \in \left[\frac{2(\delta^2 + g_{mm}^2)^3}{9\mu'_b g_{mm}^2 \delta}, \frac{2(\delta^2 + g_{mm}^2)^3}{9\mu'_b \delta^3} \right]. \quad (\text{B18})$$

In Fig. 8c, we present the transmittances as a function of the amplitude of the input field when the detuning is kept fixed within the unidirectional transport region given in Eq. (B9). We see that the lower stable branches of the bistable curves shown in Fig. 8c (the parts of the bistable curves before the bistable transitions occur) increase when we increase the intensity of the input field. This decreases the rectification, as shown in Fig. 8d.

Appendix C: Can this system be used as a phonon isolator?

In order to check the performance of the proposed system as an isolator for phonons, we study the system considering that phonons are injected in the system in both directions, that is simultaneously at the passive and active resonator sides. If the system exhibits unidirectional phonon transport under this condition, then the proposed system can be used as an isolator.

The equations of motion of the system for this case can be written as

$$\begin{aligned} \dot{b}_l &= -(\chi + i\delta_l) b_l - ig_{mm} b_g + i\varepsilon_l, \\ \dot{b}_g &= -(\chi + i\delta_g) b_g - i\mu'_b (b_g^\dagger b_g) b_g - ig_{mm} b_l + i\varepsilon_g, \end{aligned} \quad (\text{C1})$$

where the last terms on the right-hand-sides of Eq. (C1) denote the input fields. The steady-state solution of Eq. (C1) leads to

$$\bar{\mu}^2 n_g^3 - 2\bar{\mu}\bar{\Omega} n_g^2 + (\bar{\Gamma}^2 + \bar{\Omega}^2) n_g - \bar{n}_{\text{in}} = 0, \quad (\text{C2})$$

where

$$\begin{aligned} \bar{\Gamma} &= (\chi^2 + \delta_l^2 + g_{mm}^2) \chi, \quad \bar{\mu} = (\chi^2 + \delta_l^2) \mu'_b \\ \bar{\Omega} &= (\chi^2 + \delta_l^2) \delta_g - g_{mm}^2 \delta_l, \\ \bar{n}_{\text{in}} &= |\varepsilon_l|^2 g_{mm}^2 (\chi^2 + \delta_l^2) + (\chi^2 + \delta_l^2)^2 |\varepsilon_g|^2. \end{aligned}$$

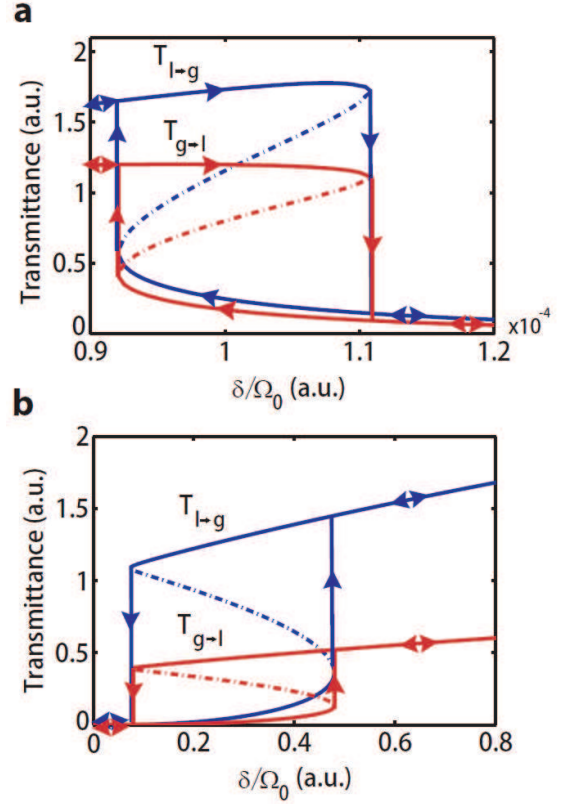


FIG. 9: (Color online). Bistability curves for the mechanical \mathcal{PT} system when phonons are input simultaneously in both directions. (a) Transmittances as functions of the detuning frequency δ when the input field amplitude is fixed at ε_d . (b) Transmittances as functions of the amplitude of the input field when the detuning frequency δ is fixed. The blue and red curves represent the power transmittance functions $T_{l \rightarrow g}$ and $T_{g \rightarrow l}$. The solid and dashed parts on each curve denote the stable and unstable solutions of the bistable systems. The unstable solutions cannot be observed in the output and thus lead to sudden transitions in the transmittance functions.

Let us first fix ε_l , ε_g , δ_g , and vary the detuning $\delta_l = \delta$. In this case, the bistable transitions for both directions occur when the detuning δ satisfies

$$\frac{\delta_g - (g_{mm}^2 \delta) / (\chi^2 + \delta^2)}{\chi(\chi^2 + \delta^2 + g_{mm}^2) / (\chi^2 + \delta^2)} = \sqrt{3}. \quad (\text{C3})$$

When the detuning is up-scanned from smaller to larger detuning values, the bistable transition occurs for

$$\begin{aligned} \delta &= \sqrt{\frac{g_{mm}^4}{4(\delta_g - \sqrt{3}\chi)^2} + \frac{(\sqrt{3}\chi^3 - \chi^2 \delta_g + \sqrt{3}g_{mm}^2 \chi)}{(\delta_g - \sqrt{3}\chi)}} \\ &\quad + \frac{g_{mm}^2}{2(\delta_g - \sqrt{3}\chi)}. \end{aligned} \quad (\text{C4})$$

When the detuning δ is down-scanned from larger to

smaller detuning values, the bistable transition occur at

$$\delta = -\sqrt{\frac{g_{mm}^4}{4(\delta_g - \sqrt{3}\chi)^2} + \frac{(\sqrt{3}\chi^3 - \chi^2\delta_g + \sqrt{3}g_{mm}^2\chi)}{(\delta_g - \sqrt{3}\chi)}} + \frac{g_{mm}^2}{2(\delta_g - \sqrt{3}\chi)}. \quad (\text{C5})$$

The transmittances presented in Fig. 9a clearly show the bistable operation. A close look at Fig. 9a reveals that the transition from the bistable region to the stable trajectories takes place at the same points for both directions. We cannot find a detuning region within which transport in one direction is allowed and the transport in the other direction is prevented. Thus, we conclude that when phonons are injected simultaneously at both input ports, we cannot see a unidirectional operation. Consequently, it is impossible to use this system as an isolator for phonons.

Let us now fix δ_l , δ_g , ε_g , and vary $\varepsilon_l = \varepsilon_d$, to check the possibility of providing a phonon isolator. The bistable transition point is just the stationary points of the function

$$\bar{f}(n_g) = \bar{\mu}^2 n_g^3 - 2\bar{\mu}\bar{\Omega} n_g^2 + (\bar{\Gamma}^2 + \bar{\Omega}^2) n_g - |\varepsilon_g|^2. \quad (\text{C6})$$

By setting $\bar{f}'(n_g) = 0$, we find

$$\bar{n}_{g1}^* = \left[2\bar{\mu}\bar{\Omega} + \sqrt{4\bar{\mu}^2\bar{\Omega}^2 - 3\bar{\mu}^2(\bar{\Gamma}^2 + \bar{\Omega}^2)} \right] (3\bar{\mu}^2)^{-1},$$

$$\bar{n}_{g2}^* = \left[2\bar{\mu}\bar{\Omega} - \sqrt{4\bar{\mu}^2\bar{\Omega}^2 - 3\bar{\mu}^2(\bar{\Gamma}^2 + \bar{\Omega}^2)} \right] (3\bar{\mu}^2)^{-1},$$

The bistable transition occurs at

$$|\varepsilon_d|^2 = \frac{f(n_{g1}^*)}{g_{mm}^2(\chi^2 + \delta_l^2)} \quad (\text{C7})$$

when the amplitude of the input field ε_d is up-scanned and for

$$|\varepsilon_d|^2 = \frac{f(n_{g2}^*)}{g_{mm}^2(\chi^2 + \delta_l^2)} \quad (\text{C8})$$

when the amplitude of the input field is down-scanned (see Fig. 9). For this case too, we do not see a unidirectional phonon transport region if we feed the inputs at the active and passive resonators sides simultaneously. Thus we conclude that although the proposed system can be used as phonon diode allowing nonreciprocal phonon transport, it cannot function as an isolator for phonons.

* Electronic address: jing-zhang@mail.tsinghua.edu.cn

† Electronic address: ozdemir@ese.wustl.edu

‡ Electronic address: yuxiliu@mail.tsinghua.edu.cn

§ Electronic address: yang@ese.wustl.edu

¶ Electronic address: fnori@riken.jp

¹ T. J. Kippenberg and K. J. Vahala, *Cavity optomechanics: back-action at the mesoscale*, Science **321**, 1172-1176 (2008).

² M. Poot and H.S.J. van der Zant, *Mechanical systems in the quantum regime*, Phys. Rep. **511**, 273-335 (2012).

³ M. Blencowe, *Quantum electromechanical systems*, Phys. Rep. **395**, 159-222 (2004).

⁴ Ya. S. Greenberg, Yu. A. Pashkin, and E. Il'ichev, *Nanomechanical resonators*, Physics-Uspekhi (Advances in Physical Sciences) **55**, 382-407 (2012).

⁵ M. Aspelmeyer, T. J. Kippenberg, and F. Marquardt, *Cavity optomechanics*, Rev. Mod. Phys. **86**, 1391-1452 (2014).

⁶ N. Li, J. Ren, L. Wang, G. Zhang, P. Hanggi, and B. Li, *Colloquium: Phononics: Manipulating heat flow with electronic analogs and beyond*, Rev. Mod. Phys. **84**, 1045-1066 (2012).

⁷ L. Wang and B. Li, *Thermal memory: a storage of phononic information*, Phys. Rev. Lett. **101**, 267203 (2008).

⁸ R. W. Andrews, R. W. Peterson, T. P. Purdy, K. Cicak, R. W. Simmonds, C. A. Regal, and K. W. Lehnert, *Bidirectional and efficient conversion between microwave and optical light*, Nature Phys. **10**, 321-326 (2014).

⁹ J. Bochmann, A. Vainsencher, D. D. Awschalom, and A. N. Cleland, *Nanomechanical coupling between microwave and optical photons*, Nature Phys. **9**, 712-716 (2013).

¹⁰ A. D. O'Connell, M. Hofheinz, M. Ansmann, R. C. Bial-

czak, M. Lenander, E. Lucero, M. Neeley, D. Sank, H. Wang, M. Weides, and J. Wenner, J. M. Martinis, and A. N. Cleland, *Quantum ground state and single-phonon control of a mechanical resonator*, Nature **464**, 697-703 (2010).

¹¹ Q. Lin, J. Rosenberg, D. Chang, R. Camacho, M. Eichenfield, K. J. Vahala, and O. Painter, *Coherent mixing of mechanical excitations in nano-optomechanical structures*, Nat. Photon. **4**, 236-242 (2010).

¹² J. Chan, T. P. Mayer Alegre, A. H. Safavi-Naeini, J. T. Hill, A. Krause, S. Gröblacher, M. Aspelmeyer, and O. Painter, *Laser cooling of a nanomechanical oscillator into its quantum ground state*, Nature **478**, 89-92 (2011).

¹³ J. D. Teufel, T. Donner, D. Li, J. W. Harlow, M. S. Allman, K. Cicak, A. J. Sirois, J. D. Whittaker, K. W. Lehnert, and R. W. Simmonds, *Sideband cooling of micromechanical motion to the quantum ground state*, Nature **475**, 359-363 (2011).

¹⁴ T. J. Kippenberg, H. Rokhsari, T. Carmon, A. Scherer, and K. J. Vahala, *Analysis of radiation-pressure induced mechanical oscillation of an optical microcavity*, Phys. Rev. Lett. **95**, 033901 (2005).

¹⁵ T. Carmon, H. Rokhsari, L. Yang, T. J. Kippenberg, and K. J. Vahala, *Temporal behavior of radiation-pressure-induced vibrations of an optical microcavity phonon mode*, Phys. Rev. Lett. **94**, 223902 (2005).

¹⁶ Y.-S. Park and H. Wang, *Resolved-sideband and cryogenic cooling of an optomechanical resonator*, Nat. Phys. **5**, 489-493 (2009).

¹⁷ C. Dong, V. Fiore, M. C. Kuzyk, and H. Wang, *Optomechanical dark mode*, Science **338**, 1609-1613 (2012).

¹⁸ M. Tomes and T. Carmon, *Photonic micro-*

- electromechanical systems vibrating at X-band (11-GHz) rates*, Phys. Rev. Lett. **102**, 113601 (2009).
- 19 J. Hofer, A. Schliesser, and T. J. Kippenberg, *Cavity optomechanics with ultrahigh-Q crystalline microresonators*, Phys. Rev. A **82**, 031804(R) (2010).
 - 20 L. Ding, C. Baker, P. Senellart, A. Lemaitre, S. Ducci, G. Leo, and I. Favero, *Wavelength-sized GaAs optomechanical resonators with gigahertz frequency*, Appl. Phys. Lett. **98**, 113108 (2011).
 - 21 M. Zhang, G. Luiz, S. Shah, G. Wiederhecker, and M. Lipson, *Eliminating anchor loss in optomechanical resonators using elastic wave interference*, Appl. Phys. Lett. **105**, 051904 (2014).
 - 22 L. Fan, K. Fong, M. Poot, H. Tang, *Cascaded optical transparency in multimode-cavity optomechanical systems*, Nat. Commun. **6**, 5850 (2015).
 - 23 C. H. Metzger and K. Karrai, *Cavity cooling of a microlever*, Nature **432**, 1002-1005 (2004).
 - 24 O. Arcizet, P.-F. Cohadon, T. Briant, M. Pinard, and A. Heidman, *Radiation-pressure cooling and optomechanical instability of a micromirror*, Nature **444**, 71-74 (2006).
 - 25 J. D. Thompson, B. M. Zwickl, A. M. Jayich, F. Marquardt, S. M. Girvin, and J.G.E. Harris, *Strong dispersive coupling of a high-finesse cavity to a micromechanical membrane*, Nature **452**, 72-75 (2008).
 - 26 R. Fleury, D. L. Sounas, C. F. Sieck, M. R. Haberman, and A. Alú, *Sound isolation and giant linear nonreciprocity in a compact acoustic circulator*, Science **343**, 516-519 (2014).
 - 27 A. A. Maznev, A. G. Every, and O. B. Wright, *Reciprocity in reflection and transmission: what is a "phonon diode"?* Wave Motion **50**, 776 (2013).
 - 28 R. Krishnan, S. Shirota, Y. Tanaka, and N. Nisguchi, *High-efficient acoustics wave rectifier*, Solid State Commun. **144**, 194 (2007).
 - 29 X.-F. Li, X. Ni, L. Feng, M.-H. Lu, C. He, and Y.-F. Chen, *Tunable unidirectional sound propagation through a sonic-crystal-based acoustic diode*, Phys. Rev. Lett. **106**, 084301 (2011).
 - 30 B. Liang, X. S. Guo, J. Tu, D. Zhang, and J. C. Cheng, *An acoustic rectifier*, Nature Materials **9**, 989 (2010).
 - 31 N. Boechler, G. Theoharis, and C. Daraio, *Bifurcation-based acoustic switching and rectification*, Nature Materials **10**, 665 (2011).
 - 32 B.-I. Popa and S. A. Cummer, *Non-reciprocal and acoustic metamaterials*, Nat. Commun. **5**, 3398 (2014).
 - 33 K. Petermann, *Laser diode modulation and noise* (Kluwer Academic, Dordrecht, 1988).
 - 34 S. R. Sklan and J. C. Grossman, *Phonon diodes and transistors from magneto-acoustics*, New J. Phys. **16** 053029 (2014).
 - 35 R. Almog, S. Zaitsev, O. Shtempluck, and E. Buks, *Noise squeezing in a nanomechanical Duffing resonator*, Phys. Rev. Lett. **98**, 078103 (2007).
 - 36 M. H. Matheny, M. Grau, L. G. Villanueva, R. B. Karabalin, M. C. Cross, and M. L. Roukes, *Phase synchronization of two anharmonic nanomechanical oscillators*, Phys. Rev. Lett. **112**, 014101 (2014).
 - 37 K. L. Ekinici and M. L. Roukes, *Nanoelectromechanical systems*, Rev. Sci. Instrum. **76**, 061101 (2005).
 - 38 I. Mahboob, E. Flurin, K. Nishiguchi, A. Fujiwara, and H. Yamaguchi, *Interconnect-free parallel logic circuits in a single mechanical resonator*, Nat. Commun. **2**, 198 (2011).
 - 39 A. N. Cleland, *Foundation of Nanomechanics -From Solid-State Theory to Device Applications* (Springer-Verlag, Berlin, 2003).
 - 40 X.-Y. Lü, J. Q. Liao, L. Tian, and F. Nori, *Steady-state mechanical squeezing in an optomechanical system via Duffing nonlinearity*, Phys. Rev. A **91**, 013834 (2014).
 - 41 K. Jacobs and A. J. Landahl, *Engineering giant nonlinearities in quantum nanosystems*, Phys. Rev. Lett. **103**, 067201 (2009).
 - 42 C. M. Bender, *Making sense of non-Hermitian Hamiltonians*, Rep. Prog. Phys. **70**, 947-1018 (2007).
 - 43 A. A. Sukhorukov, Z. Xu, and Y. S. Kivshar, *Nonlinear suppression of time reversals in \mathcal{PT} -symmetric optical couplers*, Phys. Rev. A **82**, 043818 (2010).
 - 44 H. Ramezani, T. Kottos, R. El-Ganainy, and D. N. Christodoulides, *Unidirectional nonlinear \mathcal{PT} -symmetric optical structures*, Phys. Rev. A **82**, 043803 (2010).
 - 45 Z. Lin, H. Ramezani, T. Eichelkraut, T. Kottos, H. Cao, and D. N. Christodoulides, *Unidirectional invisibility induced by \mathcal{PT} -symmetric periodic structures*, Phys. Rev. Lett. **106**, 213901 (2011).
 - 46 X. Zhu, L. Feng, P. Zhang, X. Yin, and X. Zhang, *One-way invisible cloak using parity-time symmetric transformation optics*, Opt. Lett. **38**, 2821-2824 (2013).
 - 47 C. Hang, G. Huang, and V. V. Konotop, *\mathcal{PT} symmetry with a system of three-level atoms*, Phys. Rev. Lett. **110**, 083604 (2013).
 - 48 G. S. Agarwal and K. Qu, *Spontaneous generation of photons in transmission of quantum fields in \mathcal{PT} -symmetric optical systems*, Phys. Rev. A **85**, 031802 (2012).
 - 49 H. Benisty et al. *Implementation of \mathcal{PT} symmetric devices using plasmonics: principle and applications*, Opt. Exp. **19**, 18004 (2011).
 - 50 N. Lazarides and G. P. Tsironis, *Gain-driven discrete breathers in \mathcal{PT} -symmetric nonlinear metamaterials*, Phys. Rev. Lett. **110**, 053901 (2013).
 - 51 Y. Lumer, Y. Plotnik, M. C. Rechtsman, and M. Segev, *Nonlinearly induced \mathcal{PT} transition in photonic systems*, Phys. Rev. Lett. **111**, 26390 (2013).
 - 52 A. Guo, G. J. Salamo, D. Duchesne, R. Morandotti, M. Volatier-Ravat, V. Aimez, G. A. Siviloglou, and D. N. Christodoulides, *Observation of \mathcal{PT} -symmetry breaking in complex optical potentials*, Phys. Rev. Lett. **103**, 093902 (2009).
 - 53 C. E. Rüter, K. G. Makris, R. El-Ganainy, D. N. Christodoulides, M. Segev, and D. Kip, *Observation of parity-time symmetry in optics*, Nature Phys. **6**, 192-195 (2010).
 - 54 L. Feng, M. Ayache, J. Huang, Y.-L. Xu, M.-H. Lu, Y.-F. Chen, Y. Fainman, and A. Scherer, *Nonreciprocal light propagation in a silicon photonic circuit*, Science **333**, 729-733 (2011).
 - 55 A. Regensburger, C. Bersch, M.-A. Miri, G. Onishchukov, D. N. Christodoulides, and U. Peschel, *Parity-time synthetic photonic lattices*, Nature **488**, 167-171 (2012).
 - 56 L. Feng, Y.-L. Xu, W. S. Fegadolli, M.-H. Lu, J.E.B. Oliveira, V. R. Almeida, Y.-F. Chen, and A. Scherer, *Experimental demonstration of a unidirectional reflectionless parity-time metamaterial at optical frequencies*, Nature Mater. **12**, 108-113 (2012).
 - 57 J. Schindler, A. Li, M. C. Zheng, F. M. Ellis, and T. Kottos, *Experimental study of active LRC circuits with \mathcal{PT} symmetries*, Phys. Rev. A **84**, 040101(R) (2011).
 - 58 C. Zheng, L. Hao, and G. L. Long, *Observation of fast evolution in parity-time-symmetric system*, Phil. Trans. R. Soc. A **371**, 20120053 (2013).

- ⁵⁹ S. Bittner, B. Dietz, U. Günther, H. L. Harney, M. Miski-Oglu, A. Richter, and F. Schfeär, *\mathcal{PT} symmetry and spontaneous symmetry breaking in a microwave billiard*, Phys. Rev. Lett. **108**, 024101 (2012).
- ⁶⁰ N. Bender, S. Factor, J. D. Bodyfelt, H. Ramezani, D. N. Christodoulides, F. M. Ellis, and T. Kottos, *Observation of asymmetric transport in structures with active nonlinearities*, Phys. Rev. Lett. **10**, 234101 (2013).
- ⁶¹ N. M. Chtchelkatchev, A. A. Golubov, T. I. Baturina, and V. M. Vinokur, *Stimulation of the fluctuation superconductivity by \mathcal{PT} symmetry*, Phys. Rev. Lett. **109**, 150405 (2012).
- ⁶² B. Peng, S. K. Ozdemir, F. C. Lei, F. Monifi, M. Gianfreda, G. L. Long, S. H. Fan, F. Nori, C. M. Bender, and L. Yang, *Parity-time-symmetric whispering-gallery microcavities*, Nature Phys. **10**, 394-398 (2014).
- ⁶³ L. Chang, X. Jiang, S. Hua, C. Yang, J. Wen, L. Jiang, G. Li, G. Wang, and M. Xiao, *Parity-time symmetry and variable optical isolation in active-passive-coupled microresonators*, Nature Photon. **8**, 524-529 (2014).
- ⁶⁴ C. M. Bender, B. K. Berntson, D. Parker, and E. Samuel, *Observation of \mathcal{PT} phase transition in a simple mechanical system*, Am. J. Phys. **81**, 173-179 (2013).
- ⁶⁵ X. F. Zhu, H. Ramezani, C. Z. Shi, J. Zhu, and X. Zhang, *\mathcal{PT} -symmetric acoustics*, Phys. Rev. X **4**, 031042 (2014).
- ⁶⁶ R. Fleury, D. L. Sounas, and A. Alú, *An invisible acoustic sensor based on parity-time symmetry*, Nat. Commu. **6**, 5905 (2015).
- ⁶⁷ H. Jing, S. K. Ozdemir, X.-Y. Lü, J. Zhang, L. Yang, F. Nori, *\mathcal{PT} -symmetric phonon laser*, Phys. Rev. Lett. **113**, 053604 (2014).
- ⁶⁸ X.-W. Xu, Y.-X. Liu, C.-P. Sun, Y. Li, *Mechanical \mathcal{PT} symmetry in coupled optomechanical systems*, arXiv: 1402.7221v1[quant-ph].
- ⁶⁹ See the supplementary information.
- ⁷⁰ I. V. Barashenkov, Phys. Rev. A **90**, 045802 (2014).
- ⁷¹ I. Mahboob, K. Nishiguchi, A. Fujiwara, and H. Yamaguchi, *Phonon lasing in an electromechanical resonator*, Phys. Rev. Lett. **110**, 127202 (2013).
- ⁷² E. Gil-Santos, D. Ramos, A. Jana, M. Calleja, A. Raman, and J. Tamayo, *Mass sensing based on deterministic and stochastic responses of elastically coupled nanocantilevers*, Nano Lett. **9**, 4122-4127 (2009).
- ⁷³ R. B. Karabalin, M. C. Cross, and M. L. Roukes, *Nonlinear dynamics and chaos in two coupled nanomechanical resonators*, Phys. Rev. B **79**, 165309 (2009).
- ⁷⁴ H. Okamoto, T. Kamada, K. Onomitsu, I. Mahboob, and H. Yamaguchi, *Optical tuning of coupled micromechanical resonators*, Applied Physics Express **2**, 062202 (2009).
- ⁷⁵ T. S. Biswas, J. Xu, X. Rojas, C. Doolin, A. Suhel, K.S.D. Beach, and J. P. Davis, *Remote sensing in hybridized arrays of nanostrings*, Nano Lett. **14**, 2541-2545 (2014).
- ⁷⁶ G. Anetsberger, O. Arcizet, Q. P. Unterreithmeier, R. Riviere, A. Schliesser, E. M. Weig, J. P. Kotthaus, and T. J. Kippenberg, *Near-field cavity optomechanics with nanomechanical oscillators*, Nature Phys. **5**, 909-914 (2009).
- ⁷⁷ F. Marquardt, J.G.E. Harris, and S. M. Girvin, *Dynamical multistability induced by radiation pressure in high-finesse micromechanical optical cavities*, Phys. Rev. Lett. **96**, 103901 (2006).
- ⁷⁸ H. Rokhsari, T. J. Kippenberg, T. Carmon, and K. Vahala, *Radiation-pressure-driven micro-mechanical oscillator*, Opt. Exp. **13**, 5293-5301 (2005).
- ⁷⁹ B. Peng, S. K. Özdemir, S. Rotter, H. Yilmaz, M. Liertzer, F. Monifi, C. M. Bender, F. Nori, and L. Yang, *Loss-induced suppression and revival of lasing*, Science **346**, 328-332 (2014).
- ⁸⁰ C. W. Gardiner and M. J. Collett, *Input and output in damped quantum systems: Quantum stochastic differential equations and the master equation*, Phys. Rev. A **31**, 3761-3774 (1985).
- ⁸¹ C. W. Gardiner and P. Zoller, *Quantum Noise, Third edition* (Springer-Verlag, Berlin, 2004).
- ⁸² I. V. Barashenkov and Yu. S. Smirnov, *Existence and stability chart for the ac-driven, damped nonlinear Schrödinger solitons*, Phys. Rev. E **54**, 5707 (1996).
- ⁸³ T. Herr, V. Brasch, J. D. Jost, C. Y. Wang, N. M. Konradiev, M. L. Gorodetsky, and T. J. Kippenberg, *Temporal solitons in optical microresonators*, Nat. Photon. **8**, 145 (2014).